Pinching threads, singularities and the number 0.0304...

Michael P. Brenner
Department of Mathematics, MIT, Cambridge, Massachusetts 02139

John R. Lister
DAMTP, Cambridge CB3 9EW, England

Howard A. Stone
Division of Engineering & Applied Sciences, Harvard University, Cambridge, Massachusetts 02138

(Received 7 May 1996; accepted 5 August 1996)

The dynamics of capillary pinching of a fluid thread are described by similarity solutions of the Navier–Stokes equations. Eggers [Phys. Rev. Lett. **71**, 3458 (1993)] recently proposed a single universal similarity solution for a viscous thread pinching with an inertial–viscous–capillary balance in an inviscid environment. In this paper it is shown that there is actually a countably infinite family of such similarity solutions which are each an asymptotic solution to the Navier–Stokes equations. The solutions all have axial scale $t'^{1/2}$ and radial scale t', where t' is the time to pinching. The solution obtained by Eggers appears to be special in that it is selected by the dynamics for most initial conditions by virtue of being less susceptible to finite-amplitude instabilities. The analogous problem of a thread pinching in the absence of inertia is also investigated and it is shown that there is a countably infinite family of similarity solutions with axial scale t'^{β} and radial scale t', where each solution has a different exponent β. © *1996 American Institute of Physics.*
[S1070-6631(96)02811-5]

I. INTRODUCTION

The capillary break-up of a fluid thread into smaller drops provides a simple example of a physical system which forms singularities in finite time.[1] A singularity refers to a physical quantity—such as the fluid velocity or interfacial curvature or their derivatives—that diverges to infinity. A local analysis of the fluid motion near the point where the thread pinches off is possible because the radius of the interface and the timescale of pinching become orders of magnitude smaller than any external lengthscales and timescales.[2] This separation of scales implies that the shape close to the pinch-off point may be insensitive to the details of initial conditions and external forces and would then evolve self-similarly in time.[3]

Recently Eggers[4] derived a similarity solution to a long-wavelength approximation of the Navier–Stokes equations for the radius $h(z,t)$ and axial velocity $v(z,t)$ of a thread of viscous fluid pinching off in an inviscid environment. The collapse of the thread is driven by surface tension, which generates rapidly increasing capillary pressures as the radius of the thread decreases. Gradients in the capillary pressure accelerate fluid axially against the resistance of extensional viscous stresses. The similarity solution derived by Eggers balances the effects of surface tension, inertia and viscous resistance and has the form

$$h(z,t)=\ell_\mu H\left(\frac{z-z^*}{\ell_\mu t'^{1/2}}\right)t', \tag{1}$$

$$v(z,t)=\frac{\gamma}{\mu}V\left(\frac{z-z^*}{\ell_\mu t'^{1/2}}\right)t'^{-1/2}, \tag{2}$$

where μ, ρ and γ are the viscosity, density and surface tension of the fluid, $\ell_\mu=\mu^2/(\gamma\rho)$ and $t_\mu=\mu^3/(\gamma^2\rho)$ are the natural viscous lengthscale and timescale, z^* and t^* are the location and time of pinch-off, and $t'=(t^*-t)/t_\mu$ is the dimensionless time to this singularity. The scaling functions H and V are determined as solutions to a pair of ordinary differential equations, which require three (uniquely specified) boundary conditions. The equations and boundary conditions that determine H and V do not involve any dimensional or dimensionless parameters and this leads to universal predictions for the final stages of thread pinch-off. For example, the minimum thickness of the interface h_{min} a dimensionless time t' from the singularity satisfies

$$h_{min}=\ell_\mu H^E_{min}t', \tag{3}$$

where $H^E_{min}=0.0304\ldots$ was determined numerically by Eggers and proposed to be a universal constant independent of the particular experiment. This universal law for the minimum thickness of the interface has been observed in numerical simulations and in experiments.[5,6]

The particular value of H^E_{min} has interesting consequences for the dynamics of a pinching viscous thread. In particular, because $H^E_{min}=0.0304\ldots$ is so small the similarity solution is unstable to finite-amplitude perturbations larger than a critical amplitude about $10^{-4.7}h_{min}t'^{1.5}$, which vanishes rapidly as $t'\to 0$.[7] Even thermal fluctuations in the fluid can trigger instabilities of the similarity solution, leading to a cascade of thinner and thinner necks near the pinch-off point. If the value obtained for H^E_{min} were larger (e.g., $H^E_{min}=10$), then the exponent of t' would be much less than 1.5 and this noise sensitivity would be so greatly diminished that a pinching viscous thread would be self-similar throughout the pinch-off process (until molecular scales were reached).

It is therefore of interest to pose the questions: What is the origin of the number 0.0304? How does it arise from the

Navier–Stokes equations? The goal of this paper is to answer these questions. We argue below that there are actually a *countably infinite* number of similarity solutions to the equations describing pinch-off of a viscous thread, with values of H_{min} that approximately satisfy the rule

$$H_{min}(N) \approx \frac{1}{60N-27}, \quad \text{where } N=1,2,\ldots . \tag{4}$$

The first six of these values are calculated. The number $H_{min}^{E} \approx 0.0304$ corresponds to $H_{min}(N=1) \approx 1/33$ and is the solution with the *largest* value of H_{min}. Furthermore, the shapes of the similarity solutions for different values of N are qualitatively similar, though there are quantitative differences. We conjecture that each of these similarity solutions is linearly stable before rupture. However, as with the solution obtained by Eggers (hereafter called the Eggers solution), they are all unstable to finite-amplitude instabilities. The instability for similarity solutions corresponding to $N>1$ is much more severe than for the Eggers solution. Numerical simulations show that after the stagnation point is destabilized in a similarity solution with $N>1$, the dynamics generically pushes the shape to the Eggers solution. Thus, the value $H_{min} \approx 0.0304$ is selected by the dynamics.

It is also of interest to study thread dynamics when inertial effects are small. This limit was first investigated by Papageorgiou,[8] who derived a second-kind similarity solution to a long-wavelength approximation of the Stokes equations (i.e., no inertia). This solution has the form

$$h(z,t) = \ell_R H\left(\frac{z-z^*}{\ell_R t'^{\beta}}\right) t', \tag{5}$$

$$v(z,t) = \frac{\gamma}{\mu} V\left(\frac{z-z^*}{\ell_R t'^{\beta}}\right) t'^{\beta-1}, \tag{6}$$

where $t_R = \mu \ell_R / \gamma$ is the viscous timescale based on an arbitrary lengthscale ℓ_R, and $t' = (t^* - t)/t_R$ is the dimensionless time to the singularity. The exponent β as well as the scaling functions H and V are determined from a pair of ordinary differential equations. Again we argue below that there are actually a countably infinite number of such solutions with different values of β, with that found by Papageorgiou being the solution with the largest value of β.

The paper is organized as follows. The equations governing a viscous thread with inertia are summarized in Section II and the corresponding similarity equations are derived and discussed. In Section III we describe the numerical construction of the infinite family of similarity solutions. In Section IV we address the questions of stability and selection. In Section V we turn to the equations without the inertial terms and briefly describes the construction of the infinite family of similarity solutions for this case.

II. EQUATIONS FOR A THREAD WITH INERTIA

We commence by describing the equations governing the capillary-driven collapse of an axisymmetric viscous fluid thread. Dynamical influences of the outside fluid are neglected. Under the assumption that the axial lengthscale of the thread is much greater than its radius, it may be shown that the axial velocity is nearly uniform across the thread's cross-section and that the viscous stress is dominated by the axial extension.[9–11] Thus the long-wave asymptotic expansions of the Navier–Stokes equations reduce at leading order to

$$(h^2)_t + (h^2 v)_z = 0, \tag{7}$$

$$\rho(v_t + v v_z) = -p_z + \frac{3\mu}{h^2}(h^2 v_z)_z, \tag{8}$$

where the thread has radius $h(z,t)$, axial velocity $v(z,t)$ and constant viscosity μ, density ρ and surface tension γ. Similar long-wave equations have been constructed for the pinching of a thread without viscosity[12,13] and without inertia.[8] The fluid pressure in (8) is given by

$$p = \gamma\left(\frac{1}{h} - h_{zz}\right). \tag{9}$$

The h_{zz} term in the pressure is actually asymptotically smaller than the $1/h$ term,[14] but we retain it because it has important consequences for the stability of the similarity solutions as is shown in Section IV. Additional asymptotically small corrections to the long-wave equations (7)–(9) are believed to be physically unimportant.

In the neighborhood $t' \ll 1$ of the pinch-off point, external lengthscales become irrelevant leading to a similarity solution of the form given in (1) and (2). Substituting (1) and (2) into (7)–(9) yields the ordinary differential equations

$$\frac{H'}{H} = \frac{2-V'}{2V+\eta}, \tag{10}$$

$$H^2(\eta V + V^2)' = 2H' + 6(H^2 V')', \tag{11}$$

for the scaling functions $H(\eta)$ and $V(\eta)$, where

$$\eta = \frac{z-z^*}{\ell_\mu t'^{1/2}}. \tag{12}$$

Note that the h_{zz} component of the pressure is asymptotically smaller than the other terms when $t' \ll 1$, and so does not appear in (11).

Solutions to (10) and (11) are specified by three boundary conditions. Two conditions for the desired physically relevant solutions follow from the fact that the evolution of $h(z,t)$ far away from the pinch-off point must be asymptotically much slower than that in the region around the pinch-off point. In similarity variables this requirement corresponds to the conditions of asymptotic behavior $H(\eta) \sim \eta^2$ at both positive and negative infinity. The remaining condition, which follows directly from (10), is that $V'(\eta_0) = 2$ if the solution is to be regular at any point η_0 where $2V(\eta_0) + \eta_0 = 0$. Eggers[4] showed that exactly one such η_0 exists and, guided by its role in the stability analysis of Section IV, we call it the *critical* or *stagnation* point.

These two boundary conditions at infinity are implemented numerically by guessing values of η_0 and $H_0 = H(\eta_0)$ as two initial conditions, imposing the regularity condition $V'(\eta_0) = 2$ and shooting numerically to positive and negative infinity. For most pairs (η_0, H_0) the solution does not satisfy the boundary conditions at infinity and may

not even extend to infinity. However, for every value of η_0 there are values of $H_0=H_0^f$ such that the solution on the interval $[\eta_0,\infty)$ satisfies the boundary condition $H\sim\eta^2$ at $+\infty$. We call these *forward solutions*. Similarly, for every value of η_0 there are values of $H_0=H_0^b$ such that the solution on the interval $(-\infty,\eta_0]$ satisfies $H\sim\eta^2$ at $-\infty$. We call these *backward solutions*. For most choices of η_0, $H_0^b \neq H_0^f$. However, there are particular values of η_0 where the forward and backward solution curves intersect, $H_0^b(\eta_0)=H_0^f(\eta_0)$; such a *global solution* to the similarity equations satisfies all three boundary conditions. Using a similar numerical technique, Eggers found a global solution that corresponds to the pair $(\eta_0^E,H_0^E)=(-1.5699\ldots,0.0304\ldots)$. It may be noted that H_0^E is very close to the minimum radius $H_{min}(N=1)\approx 1/33$.

To understand how these numbers arise from the ordinary differential equations (10) and (11), it is useful to examine more carefully the power-series expansions for $H(\eta)$ and $V(\eta)$ around the stagnation point $\eta=\eta_0$. Substituting expansions

$$H=\sum_{i=0}^{\infty} H_i(\eta-\eta_0)^i \quad \text{and} \quad V=\sum_{i=0}^{\infty} V_i(\eta-\eta_0)^i \tag{13}$$

into (10) and (11) yields $V'(\eta_0)=2$ and gives rise to the recurrence relations

$$3H_0^2 i(i+1)V_{i+1}+(12H_0+1)iH_i=\alpha_{i-1}, \quad i=1,2,\ldots, \tag{14}$$

$$H_0(i+1)V_{i+1}+5iH_i=\beta_i, \tag{15}$$

where α_{i-1} and β_i each depend on H_{i-1}, V_i and other lower-order coefficients. In order for a solution of these recurrence formulae to exist, the determinant of the coefficient matrix must be nonzero for all i. This criterion is violated for the ''singular'' values of H_0 given by

$$H_0(n)=\frac{1}{15n-12}, \quad n=1,2,3,\ldots. \tag{16}$$

Thus, no power-series solution to equations (10) and (11) exists for $H_0=\frac{1}{3},\frac{1}{18},\frac{1}{33},\ldots$. It is interesting to observe that the third singular value $H_0=\frac{1}{33}=0.0303\ldots$ is less than half a percent different from the numerical value H_0^E obtained by Eggers, which suggests, first, that there may be a relationship between them and, second, that there might be further solutions to (10) and (11) near the other singular values given by (16).

III. SEARCH FOR FURTHER SIMILARITY SOLUTIONS

The near-coincidence between $\frac{1}{33}$ and H_{min}^E motivated a search for other solutions near singular values of H_0 with $n\neq 3$. The numerical integration was performed by starting out at a particular (η_0,H_0) and using the series solution generated by the recurrence relations (14) and (15) to move a finite distance from η_0. This distance was chosen to be about half the local radius of convergence as estimated from $(H_i)^{-1/i}$ for i about 200, and was typically in the range 0.2–1. The equations were then integrated numerically towards positive or negative infinity using a fourth-order Runge–Kutta scheme.

As noted above, for each value of η_0 there are values of H_0 for which the solution reaches positive (or negative) infinity. A generic choice of (η_0,H_0) does not lead to a solution with $H\sim\eta^2$ but instead has either (i) $H\to\infty$ faster than exponentially or (ii) $H\to 0$ a finite distance from η_0. A closer examination of (10) and (11) shows that behavior (i) corresponds to a solution with $V\sim-\eta/2+\delta$ and $H'/H\sim 5/(4\delta)$, where $\delta\to 0$, whereas behavior (ii) corresponds to a solution with $H\sim|\eta-\eta_c|^{1/2}$ and $V\sim(\eta-\eta_c)^{-1}$, where η_c is the location of a singularity at a finite distance. Numerical solutions reaching either plus or minus infinity were identified by finding values of H_0 corresponding to the *border* between regions where the solution behaves like either (i) or (ii).

Repeating this procedure for many values of η_0 produces *curves* in the (η_0,H_0) plane corresponding either to forward solutions or to backward solutions. The desired global solutions occur at intersections between forward and backward curves. Since the equations are invariant under the transformation $\eta\to-\eta$, $V(\eta)\to-V(-\eta)$ and $H(\eta)\to H(-\eta)$, any forward (backward) solution (η_0,H_0) also has a corresponding backward (forward) solution $(-\eta_0,H_0)$. For definiteness in the following we describe only the case $\eta_0<0$.

The search for intersections is organized by noting that as H_0 tends to the singular value $H_0(n)$ given by (16) the series solution diverges (unless the linear combination of α_{n-1} and β_n corresponding to the component in the null space of the coefficient matrix happens to vanish). This observation motivates the definition

$$\nu(H_0)=(1+12H_0)/15H_0. \tag{17}$$

Singular values correspond to $\nu=n$, and we numerically

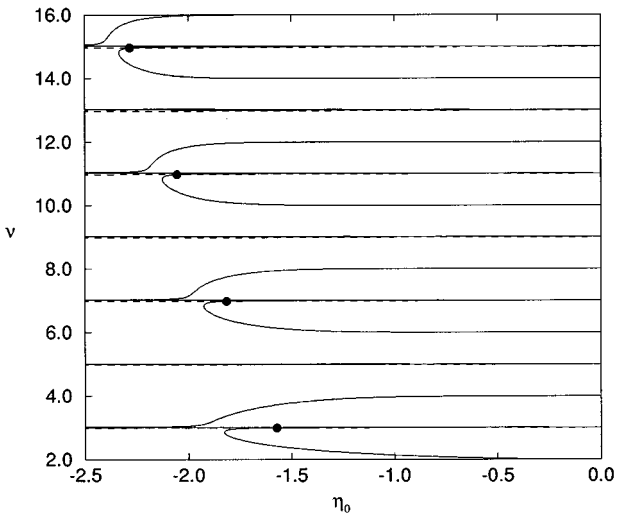

FIG. 1. The results of numerical integration from $\eta=\eta_0$, $H=H_0$, where $H_0=1/(15\nu-12)$. The solid curves are forward solutions and dashed curves are backward solutions. Intersections (solid dots) correspond to the global solutions of the equations (10) and (11). More details are shown in Fig. 2.

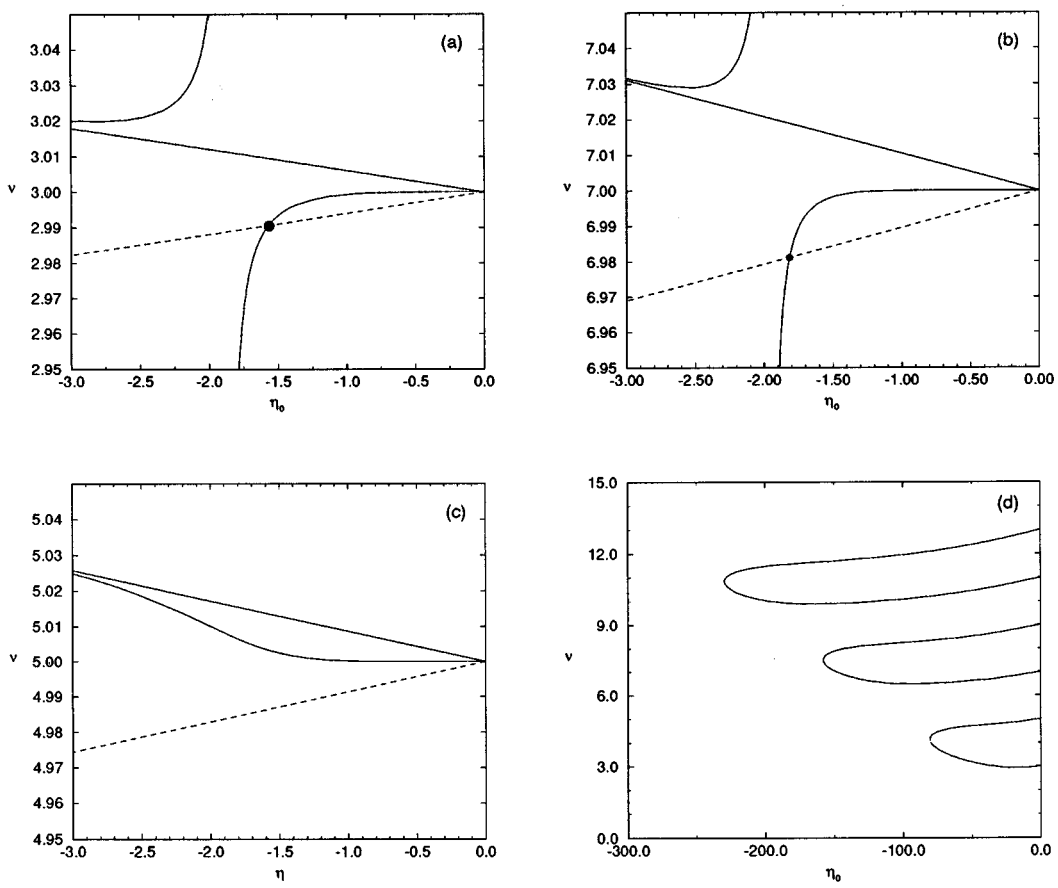

FIG. 2. (a) Blowup of Fig. 1 around $\nu=3$; (b) Blowup around $\nu=7$; (c) Blowup around $\nu=5$; (d) Global structure of the backward curves, demonstrating how they connect as $\eta_0\to-\infty$. The solid curves are forward solutions and dashed curves are backward solutions.

searched in each interval $n<\nu<n+1$. Finding forward and backward curves within any interval was initially by trial and error. The results of this search are shown in Figs. 1 and 2. Forward curves are shown as solid lines, whereas backward curves are shown as dashed lines. Four intersections, corresponding to global solutions, are shown by solid dots. Blowups of the neighborhood near the intersections around $\nu=3$ and $\nu=7$ are shown in Figs. 2(a) and 2(b). Figure 2(c) shows the neighborhood of $\nu=5$, where no intersection was found. Figure 2(d) shows backward solution curves for a much larger range of η_0, and demonstrates the global structure of the backward solutions. These figures demonstrate that a clear pattern emerges for $n\geqslant 2$, which can be summarized by the following features.

(a) As $\nu\to n$ there is one forward curve with $\eta_0 \propto |\nu-n|^{1/n}$ if n is even or $\eta_0 \propto |\nu-n|^{1/(n+1)}$ if n is odd. We denote this curve $F_n^{(1)}$.

(b) If n is odd then as $\nu\to n$ there is also one forward curve and one backward curve with $\eta_0 \propto \nu-n$. We denote these curves $F_n^{(2)}$ and B_n.

(c) $F_n^{(1)}$ lies in $(n,n+1)$ if $n=4j+1$ or $4j+2$ and in $(n-1,n)$ otherwise; F_n^2 lies in $(n,n+1)$ and B_n in $(n-1,n)$.

(d) Curve $F_{4j+3}^{(1)}$ forms a loop with $F_{4j+2}^{(1)}$. Curve $F_{4j}^{(1)}$ joins with $F_{4j-1}^{(2)}$ and $F_{4j+1}^{(1)}$ with $F_{4j+1}^{(2)}$, in a very narrow cusp which cannot be resolved numerically beyond about $\eta_0=-5$. Curves B_{4j-1} and B_{4j+1} form a long flat loop that extends to values of η_0 of order 100.

(e) There is an intersection between the $F_{4j+3}^{(1)}-F_{4j+2}^{(1)}$ loop and B_{4j+3}, which gives a global solution with $\nu\approx 4j+3$ for each j.

Statements (a) and (b) are proved by asymptotic expansion around $\nu=n, \eta_0=0$ in Appendix A; statement (c) has been shown numerically up to $n=200$; statements (d) and (e) have been shown numerically up to $\nu=15$. The similarity equations are very difficult to integrate for large ν, because of the stiffness of the ODEs and the importance of high-order coefficients in the power series near singular values. However, while (e) is not proven for arbitrarily large ν, given the

TABLE I. Values of various quantities for the first six similarity solutions.

η_0	H_0	ν	$H_{\eta\eta}(+\infty)$
−1.5699	0.030432	2.9907	4.635
−1.8140	0.010785	6.9812	105.5
−2.0537	0.006553	10.9731	545.2
−2.2821	0.004706	14.9650	1626
−2.4945	0.003672	18.9570	3673
−2.6920	0.003010	22.9490	7017
⋮	⋮	⋮	⋮

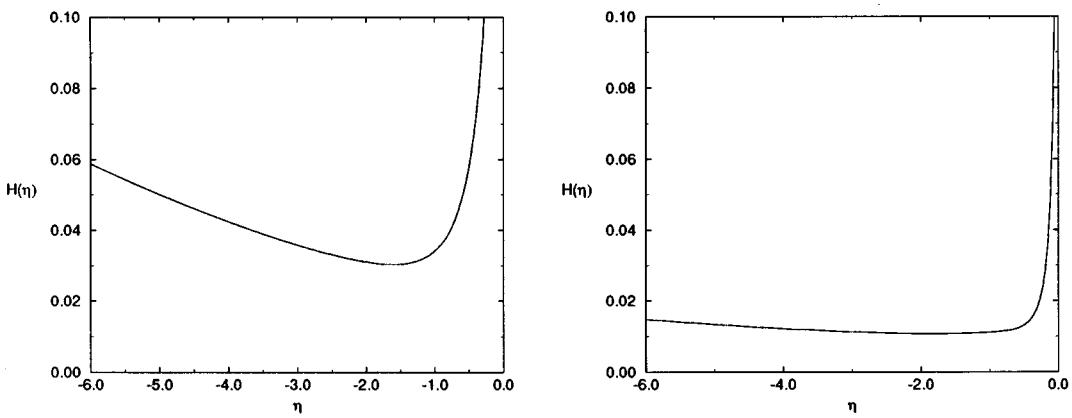

FIG. 3. Comparison of the $H(\eta)$ profiles corresponding to $\nu \approx 3$ (Eggers solution) and to the new solution with $\nu \approx 7$.

topological constraints on forward and backward curves imposed by (a)–(c), it is highly plausible that there is a countably infinite family of similarity solutions.

The Eggers solution has $\nu \approx 3$. Additional global solutions occur just below $\nu = 7,11,15,\ldots$ and are here reported for the first time, as summarized in Table I. It is interesting to note that the first six global solutions lie approximately on the straight line $\eta_0 = -(\nu + 25.1)/17.7$, which may be useful for locating higher-order solutions.

Figure 3 compares the $H(\eta)$ profiles for $\nu \approx 3$ (Eggers solution) to the new solution with $\nu \approx 7$. The solutions are qualitatively similar with a modest sloping region attached to a very steep side. The numerical values of the asymptotic curvatures for the various solutions are very different. Figure 4 compares the $V(\eta)$ profiles for these two solutions.

IV. STABILITY AND SELECTION

The results of the preceding section demonstrate that there are a countable infinity of similarity solutions to the equations describing thread pinch-off with an inertial–viscous–capillary balance. This result is unexpected since all experiments and simulations to date[4–7] have only exhibited the Eggers solution ($\nu \approx 3$), which was thought to be completely universal. With an infinity of solutions, this universality is broken, and different experiments could follow different similarity solutions. A number of questions may be posed: What is the role of the new similarity solutions? Do they have a finite basin of attraction? And why has only the Eggers solution been observed to date?

In order to address these questions, we first recall current understanding of the stability of the Eggers solution. The fact that it is observed in numerical solutions of the partial differential equations (7)–(9) leads to the reasonable conjecture that the Eggers solution is linearly stable to infinitesimal perturbations. Based on the qualitative similarity of the new solutions (Figs. 3 and 4) to the Eggers solution, we conjecture that the new solutions are also linearly stable.

It is known that the Eggers solution is unstable to finite-amplitude perturbations by a mechanism analogous to the Plateau–Rayleigh instability of a stationary liquid cylinder.[7] Perturbations of a cylinder of radius r_0 with a wavelength longer than its circumference grow by the Rayleigh mechanism on a dimensional timescale given by $6\mu r_0/\gamma$. Heuristically, we may consider the central region of the similarity solution as a cylinder of radius h_{min} and from

$$\frac{6\mu r_0}{\gamma} = \frac{6 t_\mu h_{min}}{\ell_\mu} = 6H_0(t^* - t), \tag{18}$$

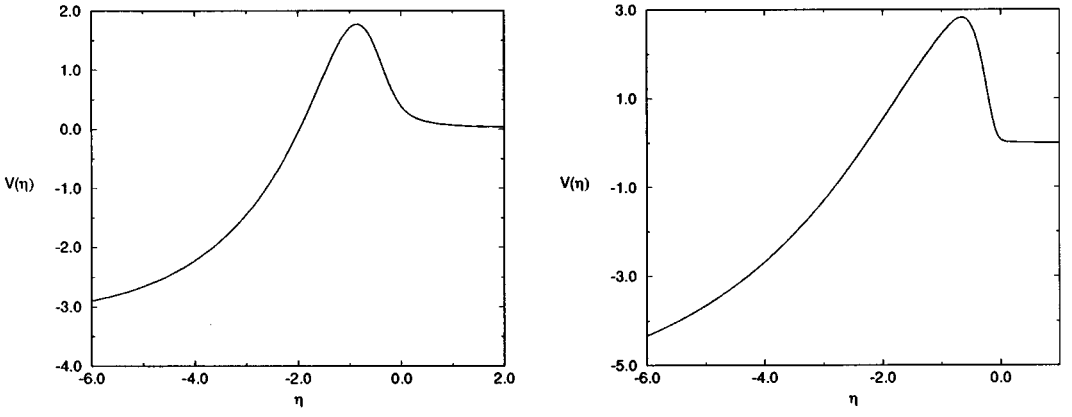

FIG. 4. Comparison of the $V(\eta)$ profiles corresponding to $\nu \approx 3$ (Eggers solution) and to the new solution with $\nu \approx 7$.

conclude that, as long as $6H_0 \ll 1$, the timescale of the Rayleigh instability is *faster* than the time to rupture and hence that the instabilities might play an important role in the dynamics. However, the other important ingredient for instability is that an unstable perturbation is not convected away from the pinching region before it has time to grow. Maximum growth is obtained for perturbations originating close to the stagnation point η_0, though this closeness is limited by the shortest wavelength perturbation that can grow. According to Plateau, the shortest unstable wavelength scales with the radius of the cylinder, and is controlled by the presence of the term h_{zz} in (9). By including this term in the analysis, it can be shown that there is a critical dimensionless amplitude for instability[7] which tends to zero at the pinch-off point roughly as $t'^{1.5}$. The effect of this instability, as seen in both experiments and calculations, is that evolution towards the Eggers solution is episodically interrupted by instability, followed by evolution back towards the Eggers solution on a finer and more local scale, thus causing the thread to exhibit a cascade of finer and finer necks (or blobs) until molecular scales are reached.[7]

In Appendix B we argue on the basis of a linear stability analysis of wave packets near the stagnation point that the new solutions are also unstable to finite-amplitude perturbations and, in any system with noise, are thus likely to be seen only transiently. For the general case the critical dimensional amplitude A_{crit} is given by

$$A_{crit} = C_\nu \ell_\mu (H_0 t'^{1/2})^\nu t', \tag{19}$$

where C_ν is a dimensionless constant and $\nu \approx 4N-1$ for the Nth solution. The critical amplitude decreases much more rapidly as $t' \to 0$ for larger values of N and the constant C_ν also decreases with N. It follows that the Eggers solution ($N=1$) is by far the least prone to instability.

We have performed extensive simulations of the partial differential equations (7)–(9) in the regime $h_{min} \ll \ell_\mu$ using a finite-difference code[7,9] modified to include a numerical viscosity term in order to damp finite-amplitude perturbations (19) associated with the mesh. Using a variety of initial conditions, we have never found a solution to converge onto one of the new similarity solutions. The solutions always converge, at least transiently and subject to the episodic instabilities described above, towards the Eggers solution. This conclusion is consistent with the previous findings that after the Eggers solution destabilizes, the interface eventually reconverges towards the Eggers solution.

Although these simulations demonstrate that the basin of attraction of the Eggers solution is larger than the basin of attraction of the new solutions, it does not rule out one of the new solutions occurring. To understand this better, we performed a simulation with the $\nu=7$ solution as the initial condition, and followed its time evolution. Because of the stability results discussed above, the solution necessarily will destabilize rapidly (even due to roundoff error). The question we wish to address is whether the solution converges back onto a new similarity solution after destabilizing, or whether it converges to the Eggers solution. The result of this simulation is shown in Fig. 5.

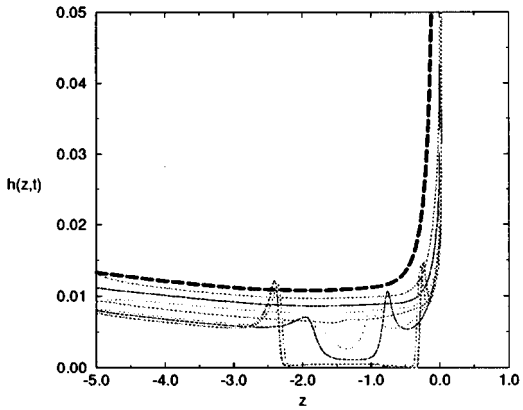

FIG. 5. Simulation starting with the $\nu \approx 7$ solution (bold dashed line) at $t=0$ and following the time evolution. The subsequent times are $t=0.1, 0.2, 0.3, 0.4, 0.5, 0.529, 0.565$, and 0.568.

The solution follows the $\nu=7$ solution for a while, suggesting linear stability, and then destabilizes as expected; the instability occurs near the stagnation point, and is the result of the finite-amplitude instability discussed above. By measuring the quantity h_{zz}, it is possible to distinguish the similarity solution towards which the simulation converges. The curvature h_{zz} away from the pinch point is time-independent, and thus provides an accurate measure of which solution occurs. For the simulation above, the maximum curvature is initially $h_{zz} \approx 105$. After the stagnation point destabilizes, the numerical solution near the breaking point has the maximum curvature $h_{zz} \approx 5$, which corresponds to the Eggers solution (Table I).

In repeated simulations of this type, it was always found that the destabilization of the stagnation point leads to the Eggers solution. This behavior can be rationalized: After the destabilization, the flat part of the similarity solution steepens until it reaches an allowable value of the asymptotic curvature (given by the similarity solutions). Since the *smallest* asymptotic curvature corresponds to the Eggers solution, this curvature will be reached first during the steepening. Thus, destabilization of a flat region generically leads to the Eggers solution.

V. EQUATIONS FOR A THREAD WITHOUT INERTIA

We turn now to similarity solutions for the pinching of a thread under conditions in which inertia is negligible, a problem first considered by Papageorgiou.[8] Substitution of (5) and (6) into (7)–(9), while neglecting the inertial terms in (8), yields the ordinary differential equations

$$\frac{H'}{H} = \frac{2-V'}{2V+2\beta\eta}, \tag{20}$$

$$H' + 3(H^2 V')' = 0, \tag{21}$$

for the scaling functions $H(\eta)$ and $V(\eta)$, where now

$$\eta = \frac{z-z^*}{\ell_R t'^\beta}. \tag{22}$$

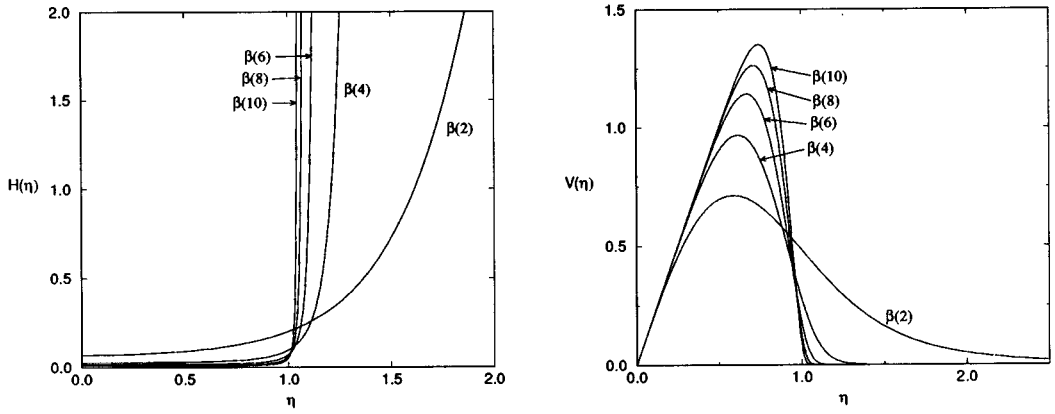

FIG. 6. Comparison of the $H(\eta)$ and $V(\eta)$ profiles for different values of β.

The exponent β remains to be determined, and so this similarity solution is of the second kind.[3] One boundary condition for (20) and (21) is analogous to that for the inertial similarity equations (10) and (11), namely that $V'(\eta_0)=2$ at the point η_0 where $V(\eta_0)+\beta\eta_0=0$. The general asymptotic behavior of (20) and (21) as $\eta\to\pm\infty$ is $H \propto \eta^{1/\beta}$ and $V\to V_{\pm\infty}$, where $V_{\pm\infty}$ are constants. The remaining two boundary conditions are thus $V_{+\infty}=V_{-\infty}=0$, which correspond to the requirement that the flow is driven locally by capillary pinching and not by an imposed axial tension $3\mu h^2 v_z$ at infinity.

We note that it is possible to integrate (20) once, then eliminate V and integrate twice more to obtain successively

$$H+3H^2V'=3k, \tag{23}$$

$$\frac{(1-\beta)H^2+\frac{1}{3}H-k/2}{\left(H+\frac{1}{2}k/H_0\right)(H-H_0)}\times\frac{H'}{H}=\frac{H''}{H'}, \tag{24}$$

$$\int_{H_0}^{H}\frac{\left(x+\frac{1}{2}k/H_0\right)^{\beta+1-1/m}dx}{x(x-H_0)^{1-1/m}}=K(\eta-\eta_0), \tag{25}$$

where

$$H_0=H(\eta_0),\ 3k=H_0+6H_0^2,\ m=\frac{1+12H_0}{6(2+\beta)H_0}, \tag{26}$$

and K is an arbitrary constant. Since the equations are invariant under $\eta\to\lambda\eta$, $V\to\lambda V$, the constant K could be set to 1 if desired. While it is satisfying to be able to perform these integrations (as computed by Papageorgiou for the case $m=2$), it is actually again more instructive to consider power-series solutions around $\eta=\eta_0$.

We observe first that $H=H_0$, $V=2(\eta-\eta_0)$ is an exact solution of (20) and (21) and so the recurrence relations

$$3H_0^2 i(i+1)V_{i+1}+(12H_0+1)iH_i=\alpha_{i-1},\quad i=1,2,\ldots, \tag{27}$$

$$H_0(i+1)V_{i+1}+2(2+\beta)iH_i=\beta_i, \tag{28}$$

have, in general, only the trivial solution $H_i=V_{i+1}=0$ for $i\geqslant 1$. Thus for these equations we actually need the determinant of the coefficient matrix to vanish for some i if a nontrivial solution is to exist. If this occurs for $i=m$ then we find that

$$H_0=\frac{1}{6(2+\beta)m-12},\quad H=\sum_{j=0}^{\infty}H_{mj}(\eta-\eta_0)^{mj}$$

$$\text{and}\quad V=\sum_{j=0}^{\infty}V_{mj+1}(\eta-\eta_0)^{mj+1}, \tag{29}$$

where H_m is arbitrary (and can be set to 1 by variable rescaling), and $H_{mj}, V_{mj+1}\propto H_m^j$ Starting with these series, we can integrate (20) and (21) numerically and determine $V_{\pm\infty}(m,\beta)$. The boundary conditions $V_{\pm\infty}=0$ are found to require that m is even and $\eta_0=0$, and that β is a function of m. The solution found by Papageorgiou is $\beta(2)\approx 0.175$, but there is a solution for each even value of m. Some of these and the values of $\beta(m)$ are shown in Figs. 6 and 7.

As m increases and the solutions become flatter near $\eta=0$, $\beta(m)$ decreases and so the shapes $H \propto \eta^{1/\beta}$ become steeper away from $\eta=0$. It may be expected from the inertial case, and is confirmed in Appendix B, that solutions with large values of m will be linearly stable but very prone to a finite-amplitude version of the Rayleigh instability. We also note that it is easy to show that the continued neglect of the inertial terms as $t'\to 0$ requires $\beta>\frac{1}{2}$ and so all of these solutions will eventually enter the inertial regime.

VI. CONCLUSIONS

In this paper we have constructed numerically two infinite families of similarity solutions for capillary pinching of a fluid thread, corresponding to the presence and the absence of inertia. The former case, which extends previous work of Eggers, gives rise to first-kind similarity solutions with the same time-dependence, and the latter, which extends the work of Papageorgiou, gives rise to second-kind similarity solutions each of which has a different time-dependence.

It is interesting that there are multiple similarity solutions since only the solution determined by Eggers has been

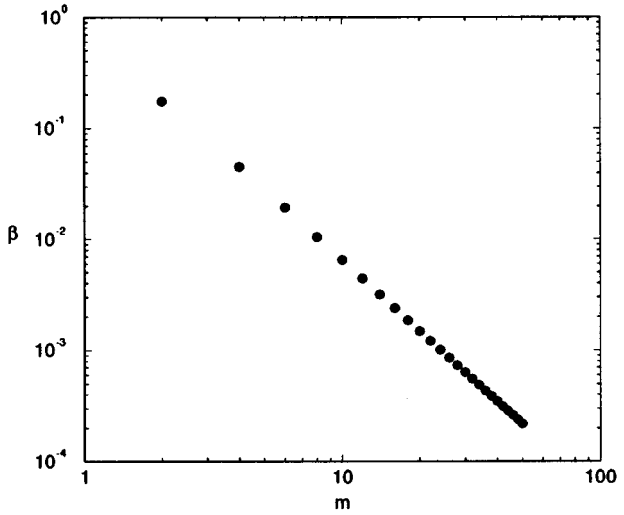

FIG. 7. Variation of the similarity exponent β with the index m of the power-series about $\eta=\eta_0$. Over the range shown there is an approximate fit $\beta \propto m^{-2.1}$.

seen in previous numerical and experimental studies. As demonstrated here, the similarity solutions are unstable to finite-amplitude perturbations and the Eggers solution is special because it is the least unstable. Through numerical simulations, we have shown that the destabilization of the new similarity solutions leads directly to the Eggers solution. We rationalize this behavior by proposing a selection principle for the similarity solutions: namely, a flat thread will steepen until it reaches the smallest possible curvature consistent with the similarity solutions.

Finally, we comment on the huge asymmetry and the small dimensionless minimum width of both the Eggers solution and the new inertial solutions. From our analysis, these properties are related to the fact that global solutions to the similarity equations are only found very close to certain values of H_0 at which the series solution is singular owing to a sort of degeneracy or resonance between the continuity and momentum equations at the stagnation point. The physical significance of these intriguing singularities is not clear.

ACKNOWLEDGMENTS

We thank S. R. Nagel for useful discussions. HAS thanks the ACS Petroleum Research Fund for support through Grant No. 28690-AC9. MPB thanks the NSF for a postdoctoral fellowship.

APPENDIX A: ASYMPTOTICS

The purpose of this appendix is to derive asymptotic results about the solutions of (10) and (11) when H_0 is close to the singular values (16) or, equivalently, when $\nu(H_0)=(1+12H_0)/15H_0$ is close to an integer value n. These results form the basis for statements (a)–(c) in Section III.

We commence with an examination of the power series (13) as $\nu \to n$. Elimination of V_{i+1} from the recurrence relations (14) and (15) yields

$$H_i=\frac{\gamma_i H_0}{\nu-i}, \quad \text{where} \quad \gamma_i(\nu,\eta_0)=\frac{i^{-1}\alpha_{i-1}-3\beta_i H_0}{15H_0^2} \tag{A1}$$

can be found as a rational function of ν and η_0. It follows that, except in the special case that $\gamma_n(n,\eta_0)=0$, there are no regular solutions when $\nu=n$ with n an integer, since the series breaks down at $i=n$. Motivated by this observation, we define $\epsilon(\nu)=(\nu-n)/\gamma_n(\nu,\eta_0)$. There are two possibilities as $\nu \to n$.

The first possibility is that $\epsilon \to 0$, as will certainly happen if $\gamma_n(n,\eta_0) \neq 0$. In this case, consideration of the way that H_n appears in α_i and β_i for $i>n$ shows that $h_n,\ldots,h_{2n-1},u_{n+1},\ldots,u_{2n}=O(\epsilon^{-1})$, $h_{2n},\ldots,h_{3n-1},u_{2n+1},\ldots,u_{3n}=O(\epsilon^{-2})$, etc., as $\epsilon \to 0$. Motivated by this observation, we define rescaled variables by

$$y=\epsilon^{-1/n}(\eta-\eta_0) \quad \text{and} \quad W(y)=\epsilon^{-1/n}\left(V(\eta)+\frac{1}{2}\eta_0\right) \tag{A2}$$

so that H and W/y become power series in y^n as $\epsilon \to 0$. We analyze this case, which leads to statement (a), below.

The second possibility is that $\gamma_n(\nu,\eta_0) \to 0$ as $\nu \to n$ in such as a way that $\epsilon \not\to 0$. The most important example of this is when n is an odd integer and $\eta_0 \to 0$ as $\epsilon \to 0$. The series solution to (10) and (11) has the property, arising from the reflectional symmetry of the differential equations, that the coefficients H_{2i} and V_{2i+1} are even functions of η_0, while H_{2i+1} and V_{2i} are odd functions of η_0. Thus if n is odd then $\gamma_n(n,\eta_0)=O(\eta_0)$ as $\eta_0 \to 0$ and hence $H_n=O(\eta_0/(\nu-n))$ in the joint limit $\eta_0 \to 0$ and $\nu \to n$. It follows that H and V/η can be written asymptotically as joint power series in x^2 and $\eta_0 x^n/(\nu-n)$, where $x=\eta-\eta_0$, whose coefficients depend only on n and not on η_0. It is highly plausible, and can be confirmed numerically, that if a large positive value of $\eta_0/(\nu-n)$ gives solution behavior (i) on forward integration, then a large negative value will give behavior (ii), and vice versa. It follows that a suitable intermediate value of $\eta_0/(\nu-n)$ will give a forward curve and hence that the negative of this value will give a backward curve. This argument leads to statement (b).

Returning to the first possibility and making the substitution (A2), we find that

$$H'+3(H^2W')'=O(\epsilon^{1/n}), \tag{A3}$$

$$(2W+y)H'+(W'-2)H=0, \tag{A4}$$

which can be integrated numerically from initial conditions

$$H=\frac{1}{15n-12}(1+y^n+\cdots)$$

and

$$W=y\left(2-\frac{5n}{n+1}y^n+\cdots\right), \tag{A5}$$

near $y=0$. We note that (A3) and (A4) are invariant under the transformations $y \to y+2w_\infty$, $W \to W-w_\infty$ and $y \to Py$,

$W \to PW$ for any constants w_∞ and P. It is then straightforward to show that the asymptotic behavior of (A3) and (A4) as $y \to \infty$ can be written in the form

$$H = P^2(y+2w_\infty)^2 + \frac{1}{2} + \frac{6a-1}{24P^2(y+2w_\infty)^2} + O(y+2w_\infty)^{-4}, \tag{A6}$$

$$PW = Pw_\infty + \frac{1}{3P(y+2w_\infty)} + \frac{a}{P^3(y+2w_\infty)^3} + O(y+2w_\infty)^{-5}, \tag{A7}$$

where the three constants $P(n)$, $w_\infty(n)$ and $a(n)$ must be determined numerically by integrating from the initial conditions (A5). The expressions (A6) and (A7) are not uniformly valid, but must be matched onto solutions of (10) and (11) when $y = O(\epsilon^{-1/n})$. In preparation for matching we note that

$$V \sim -\frac{1}{2}\eta_0 + \epsilon^{1/n} w_\infty, \quad H \sim \epsilon^{-2/n} P^2 x^2 \ \text{ in } \ \epsilon^{1/n} \ll x \ll 1, \tag{A8}$$

where $x = \eta - \eta_0$.

Now $H \propto x^2$, $x \gg V + \frac{1}{2}\eta_0$ is a consistent asymptotic for (11). Substituting this asymptotic into (10) at leading order, we obtain

$$x^4 (Vx)' \sim 6(x^4 V')'. \tag{A9}$$

Most solutions of (A9) have $V = O[x^{-1} \exp(x^2/12)]$ as $x \to \infty$. If we are to obtain the exceptional, but desired, behavior $V = O(x^{-1})$ then V must satisfy $V \sim A + Bx^{-3}$ as $\eta \to 0$, where A/B is a certain $O(1)$ number that could be determined by numerical integration. Since (A8) shows that $B = o(\epsilon^{1/n})$, we must also have $-\frac{1}{2}\eta_0 + \epsilon^{1/n} w_\infty = o(\epsilon^{1/n})$, i.e., $\eta_0 \sim 2\epsilon^{1/n} w_\infty$ as $\epsilon \to 0$. Recalling that $\gamma_n(n, \eta_0) = O(\eta_0)$ when n is odd, we have arrived at an explanation and means of calculation of forward curves with $\eta_0 = O(\nu - n)^{1/n}$ when n is even and $\eta_0 = O(\nu - n)^{1/(n+1)}$ when n is odd, thus justifying statement (a). Whether these forward curves lie in $\nu > n$ or $\nu < n$ is determined by the sign of γ_n, and the pattern of signs of γ_n that gives rise to statement (c) has been verified numerically up to $n = 200$.

APPENDIX B: STABILITY ANALYSIS

We wish to study the stability of similarity solutions to (7) and (8). Our analysis is similar to that of Brenner *et al.*,[7] but differs both in the form of the asymptotic expansion and in correcting some minor algebraic errors. We commence by writing

$$h = \ell_\mu \{H(\eta) + \delta g(\eta, t')\} t', \tag{B1}$$

$$v = \frac{\ell_\mu}{t_\mu} \{V(\eta) + \delta u(\eta, t')\} t'^{-1/2}, \tag{B2}$$

where $H(\eta)$ and $V(\eta)$ satisfy the similarity equations (10) and (10), and δ is a small parameter. We substitute into (7) and (8), retaining terms to $O(\delta)$, and obtain

$$\partial_\tau g - g + \left(V + \frac{\eta}{2}\right) g_\eta + \frac{1}{2} H u_\eta + H_\eta u + \frac{1}{2} V_\eta g = 0, \tag{B3}$$

$$\partial_\tau u + \frac{1}{2}u + \left(V + \frac{\eta}{2}\right) u_\eta + u V_\eta - 3u_{\eta\eta} + \frac{6H_\eta V_\eta g}{H^2} - \frac{6V_\eta g_\eta}{H} - \frac{6H_\eta u_\eta}{H} - \frac{g_\eta}{H^2} + \frac{2H_\eta g}{H^3} - t' g_{\eta\eta\eta} = 0, \tag{B4}$$

where $\tau = -\ln(t')$. We have omitted a term $t' H_{\eta\eta\eta}/\delta$ from (B4) on the grounds that it corresponds to a small (relative to H) global adjustment to the similarity solution, but does not affect the stability. We have also continued to omit various $O(t')$ terms from (B3) and (B4) that arise as asymptotically small corrections to the long-wave expansion in (7)–(9) since these are believed to be physically unimportant; as shown below, the $t' g_{\eta\eta\eta}$ term simply establishes a long-wave cutoff and does not affect the dynamics of disturbance amplification.

After accounting for the different scalings of the axial and radial lengthscales, the radius of the thread is $Ht'^{1/2} \ll 1$ in η-space. Since we expect instabilities to correspond to a form of the Rayleigh instability, we consider disturbances with wavelength $O(\epsilon)$, where $Ht'^{1/2} \leqslant \epsilon \ll 1$. Equations (B3) and (B4) have two τ-derivatives and thus support two modes of disturbance: simple scalings show that one corresponds to viscous damping of disturbance inertia and has a decay rate $O(\epsilon^{-2})$; the other is the Rayleigh mode we are interested in and has a frequency $O(\epsilon^{-1})$. Accordingly, a suitable adaptation of the WKB method is to write

$$\begin{pmatrix} g \\ u \end{pmatrix} = \begin{pmatrix} G(\eta,\tau) \\ U(\eta,\tau) \end{pmatrix} \exp\left[\frac{\mathrm{i}\Theta(\eta,\tau)}{\epsilon}\right] + O(\epsilon), \tag{B5}$$

where Θ is $O(1)$. The local wavenumber and frequency are given by

$$k = \Theta_\eta/\epsilon \quad \text{and} \quad \omega = -\Theta_\tau/\epsilon. \tag{B6}$$

Substituting (B5) into (B3) and (B4) gives

$$\left(\frac{\mathrm{i}\Theta_\tau}{\epsilon} + \left(V + \frac{\eta}{2}\right)\frac{\mathrm{i}\Theta_\eta}{\epsilon} + \frac{1}{2}V_\eta - 1\right) G + \frac{\mathrm{i}\Theta_\eta}{2\epsilon} H U + G_\tau + \left(V + \frac{\eta}{2}\right) G_\eta = O(U), \tag{B7}$$

$$\frac{\Theta_\eta^2}{\epsilon^2} 3U - \frac{\mathrm{i}\Theta_\eta}{\epsilon}\left(\frac{6V_\eta}{H} + \frac{1}{H^2} - (\epsilon^{-2}t')\Theta_\eta^2\right) G = O(G, \epsilon^{-1}U). \tag{B8}$$

(The damped inertial mode corresponds to a balance $(3\Theta_\eta^2/\epsilon^2 + \mathrm{i}\Theta_\tau/\epsilon)U \sim 0$ in (B8) but requires a rescaling of the variables with $\Theta_\tau = O(\epsilon^{-1})$ for further asymptotic analysis.)

Equations (B7) and (B8) allow the evolution of the Rayleigh mode to be evaluated. From (B8) we first obtain

$$U = \frac{2\mathrm{i}\epsilon}{\Theta_\eta H}\left(V_\eta + \frac{1 - (\epsilon^{-2}t')H^2\Theta_\eta^2}{6H}\right) G, \tag{B9}$$

so that $U=O(\epsilon G)$. Equation (B7) then reduces at $O(\epsilon^{-1})$ to $\Theta_\tau+(V+\frac{1}{2}\eta)\Theta_\eta=0$ or

$$\omega=\left(V+\frac{1}{2}\eta\right)k, \tag{B10}$$

which may be differentiated with respect to η to give

$$k_\tau+\left(V+\frac{1}{2}\eta\right)k_\eta=-\left(V_\eta+\frac{1}{2}\right)k. \tag{B11}$$

Finally, we use (B9) to eliminate U from (B7) at $O(1)$ and obtain the evolution equation

$$G_\tau+\left(V+\frac{1}{2}\eta\right)G_\eta=\left\{\frac{1-k^2H^2t'}{6H}+\frac{1}{2}V_\eta+1\right\}G. \tag{B12}$$

Equations (B10)–(B12) are readily interpreted. The phase velocity ω/k and the group velocity are both equal to the sum V^* of the interfacial velocity V and the pseudo-velocity $\frac{1}{2}\eta$ induced by the time-dependent definition of η. Moving with this effective velocity V^*, the local wavelength is stretched by the divergence of the effective velocity, and the local growth rate is the sum of the long-wave Rayleigh growth rate, growth due to necking of the thread under extension, and a pseudo-growth due to the time-dependent radial scaling. We can, moreover, integrate both (B11) and (B12) along characteristics of V^* to obtain

$$\frac{k(\eta(\tau),\tau)}{k(\eta_1,\tau_1)}=\frac{V^*(\eta_1)}{V^*(\eta(\tau))}. \tag{B13}$$

$$\frac{G(\eta(\tau),\tau)}{G(\eta_1,\tau_1)}=\exp\left\{\int_{\eta_1}^{\eta(\tau)}\left(\frac{1-k(\eta)^2H^2t'}{6H}+\frac{1}{2}V_\eta+1\right)\frac{d\eta}{V^*}\right\}, \tag{B14}$$

where $\eta(\tau)$ is obtained by solving $\eta_\tau=V^*(\eta)$ subject to $\eta(\tau_1)=\eta_1$.

Consideration of (B13) and (B14) shows that the most dangerous perturbation is one with initial wavelength $k^{-1}(\eta_1)=Ht'^{1/2}$ starting with η_1 close to the stagnation/critical point η_0 where $V^*(\eta_0)=0$ that was introduced earlier. Growth is dominated by the region $|\eta_1-\eta_0|\ll|\eta-\eta_0|\ll1$ in which Taylor expansion of the integrand of (B14) gives

$$\frac{(6H_0)^{-1}+\frac{1}{2}V_\eta(\eta_0)+1}{(\eta-\eta_0)V_\eta^*(\eta_0)}=\frac{\nu}{\eta-\eta_0}, \tag{B15}$$

on using $H_0=(15\nu-12)^{-1}$, $V_\eta(\eta_0)=2$, $V^*(\eta_0)=0$ and $V_\eta^*(\eta_0)=\frac{5}{2}$. It follows that the amplitude of a disturbance originating at $\eta=\eta_1$ grows by a factor proportional to $|\eta_1-\eta_0|^{-\nu}$ by the time it reaches $\eta=O(1)$. If the final amplitude is $O(1)$ then we assume somewhat heuristically that the original similarity solution has become unstable to the formation of a secondary ''neck'' or ''blob,'' though the initial linearization about H and V is, of course, invalid by this stage. Noting that our implicit assumption of a localized wave packet requires $|\eta_1-\eta_0|\geqslant O(k^{-1})=O(H_0t'^{1/2})$, we conclude that the critical initial amplitude for instability has the form

$$G_{crit}=C_\nu\left(\frac{t'^{1/2}}{15\nu-12}\right)^\nu, \tag{B16}$$

where C_ν is a constant that must be determined numerically. In dimensional units, this result may be expressed as a critical amplitude $A_{crit}=\ell_\mu G_{crit}t'$. As $t'\to0$, the new similarity solutions with $\nu\approx7,11,15,\ldots$ are clearly much less stable than the solution with $\nu\approx3$ found by Eggers.

Finally, we note that the WKB analysis [equations (B7) and (B8)] only involves the viscous terms at leading order. Thus, the same analysis may be applied to a thread pinching in the absence of inertia after accounting for the different time dependence (t^β) of the similarity solution. We find that equations (B13) and (B14) are unchanged save for the redefinition of the phase and group velocity as $V^*=V+\beta\eta$ and the replacement of t' in (B14) by $t'^{(2-2\beta)}$. Then, for the inertialess problem (B15) becomes

$$\frac{(6H_0)^{-1}+\frac{1}{2}V_\eta(\eta_0)+1}{(\eta-\eta_0)V_\eta^*(\eta_0)}=\frac{m}{\eta-\eta_0}. \tag{B17}$$

The time dependence of the similarity solution means now that a localized wave packet has a size $O(H_0t'^{(1-\beta)})$ in η-space, and so the critical dimensional amplitude for instability has the form

$$G_{crit}=C_m\ell_R(H_0t'^{(1-\beta)})^mt', \tag{B18}$$

where H_0 depends on the scaling exponent β as given in equation (26). Therefore, similarity solutions with larger m, corresponding to smaller β, are much less stable than the solution with $\beta(2)$ determined by Papageorgiou.[8]

[1] R. E. Caflisch and G. C. Papanicolaou, *Singularities in Fluids, Plasmas, and Optics*, Volume C404 of NATO ASI Series (Kluwer Academic, New York, 1993).

[2] J. Keller and M. J. Miksis, ''Surface tension driven flows,'' SIAM J. Appl. Math. **43**, 268 (1983).

[3] G. I. Barenblatt, *Similarity, Self-Similarity, and Intermediate Asymptotics* (Consultants Bureau, New York, 1979).

[4] J. Eggers, ''Universal pinching of 3D axisymmetric free-surface flow,'' Phys. Rev. Lett. **71**, 3458 (1993).

[5] X. D. Shi, M. P. Brenner, and S. R. Nagel, ''A cascade of structure in a drop falling from a faucet,'' Science **265**, 219 (1994).

[6] T. A. Kowalewski, ''On the separation of droplets from a liquid jet,'' Fluid Dyn. Res. **17**, 121 (1996).

[7] M. P. Brenner, X. D. Shi, and S. R. Nagel, ''Iterated instabilities during droplet fission,'' Phys. Rev. Lett. **73**, 3391 (1994).

[8] D. Papageorgiou, ''On the breakup of viscous liquid threads,'' Phys. Fluids **7**, 1529 (1995).

[9] J. Eggers and T. F. Dupont, ''Drop formation in a one-dimensional approximation of the Navier–Stokes equation,'' J. Fluid Mech. **262**, 205 (1994).

[10] J. Eggers, ''Theory of drop formation,'' Phys. Fluids **7**, 941 (1995).

[11] S. Bechtel, J. Cao, and M. G. Forest, ''Closure to all orders in 1–d models for slender viscoelastic free jets: An integrated theory for axisymmetric, torsionless flows,'' Stability Appl. Anal. Continuous Media **2**, 59 (1992).

[12] H. C. Lee, ''Drop formation in a liquid jet,'' IBM J. Res. Dev. **18**, 364 (1974).

[13] L. Ting and J. B. Keller, ''Slender jets and thin sheets with surface tension,'' SIAM J. Appl. Math. **50**, 153 (1990).

[14] S. E. Bechtel, C. D. Carlson, and M. G. Forest, ''Recovery of the Rayleigh capillary instability from slender 1–d inviscid and viscous models,'' Phys. Fluids **7**, 2956 (1995).